International Journal of Engineering Trends and Technology
ISSN: 2231 – 5381 / https://doi.org/10.14445/22315381/IJETT-V70I5P206

Volume 70 Issue 5, 37-45, May 2022
© 2022 Seventh Sense Research Group®

*Original Article*

# Theoretical Modelling and Simulation of Circular Diaphragm-based Comb Drive Capacitive Pressure Sensor (CD-CDCPS)

Maibam Sanju Meetei[1], Heisnam Shanjit Singh[2], Rakesh Sharma[1], Ningthoukhongjam Vikimchandra Singh

*[1] Electronics and Communication Engineering, Rajiv Gandhi University, Arunachal Pradesh, India.*
*[2]Physics, Rajiv Gandhi University, Arunachal Pradesh, India.*
*[3]Statistics, Rajiv Gandhi University, Arunachal Pradesh, India.*

[1]maibam.meetei@rgu.ac.in

Received: 27 January 2022 Revised: 06 April 2022 Accepted: 28 April 2022 Published: 19 May 2022

***Abstract*** - *The mathematical modeling and simulation of circular diaphragm-based comb drive pressure is demonstrated in this work. The fundamental configurations of capacitors for use as sensors are discussed. A step-by-step design flow process is established for building a diaphragm-based comb-drive capacitive pressure sensor. The modeling is divided into two parts: mechanical and electrostatic. In mechanical, the deflection of the circular diaphragm is calculated, and in electrostatic, the change in capacitance is formulated rather than the absolute capacitance because finding the absolute capacitance for such a complex structure is extremely difficult. The sensor's 3D model is simulated in the COMSOL Multiphysics simulator, confirming the mathematically determined result. Physical dimensions of the diaphragm and inter-digited finger of the comb, Young's modulus, and Poison's ratio of the diaphragm material are among the factors that can improve CD-CDCPS sensitivity. For a diaphragm thickness of 25 µm, the sensitivity of the circular diaphragm-based comb-drive capacitive pressure for simulated and calculated is 0.192 fF/MPa and 0.235 fF/MPa, respectively.*

***Keywords*** - *Comb-drive, Deflection, Linearity, Sensitivity, Touch-mode, Sensitivity.*

## 1. Introduction

A capacitor becomes an indispensable part of most electronic devices because of its charge storing capacities and its properties in sensing signal processing parameters. In various literature [1]-[4], many authors have used the preliminary definition of the capacitance (C) of a capacitor which is influenced by the length (*l*), breath (*b*), the separation (*d*) between two parallel plates, and the dielectric coefficient (*ε*) of the dielectric material between parallel plates. Mathematically, we write as:

$$C = \varepsilon \frac{lb}{d}. \quad (1)$$

Whereas a parallel plate capacitor is used to produce a sensor by making one or more parameters a function of stimulation. A basic parallel capacitor can be used as a sensor in three different ways:

Horizontal overlapping area change: The overlapping area of a simple parallel plate capacitor can be altered by horizontally sliding one of the plates. The plate can be shifted in either a lengthwise or a widthwise direction. Fig. 1 shows the capacitive sensor by changing the overlapping areas. The mathematical expression of change in capacitance is given by

$$\Delta C = \varepsilon \frac{(l-x)b}{d}. \quad (2)$$

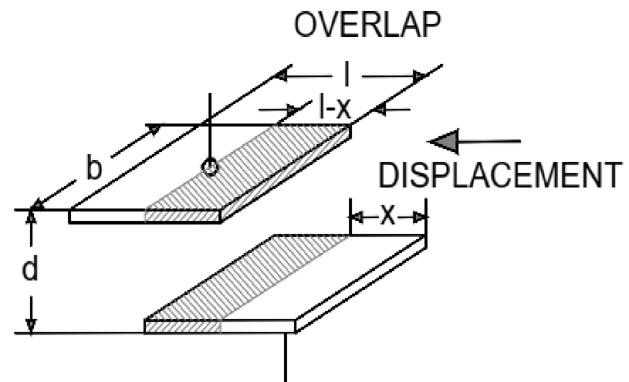


**Fig. 1 Capacitive sensor by changing the overlapping areas**

This is an open access article under the CC BY-NC-ND license (http://creativecommons.org/licenses/by-nc-nd/4.0/)

Vertical spacing between plates can be adjusted by vertically shifting one of the plates in a simple parallel plate capacitor. The plate can be moved up and down in a vertical direction. The change in vertical distance outward is depicted in fig. 2. The change in capacitance produced by vertical plate movement is

$$\Delta C = \varepsilon \frac{lb}{(d-x)} . \quad (3)$$

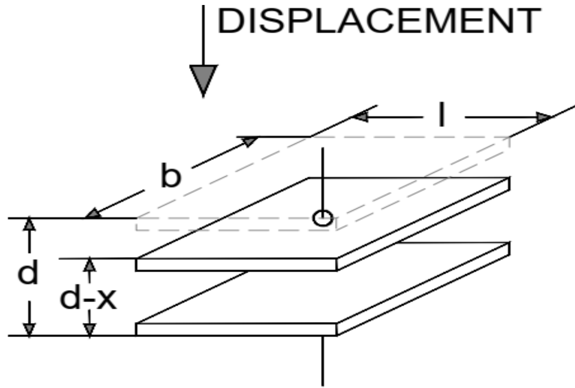


**Fig. 2 Capacitive sensor by changing the vertical plate movement**

An external force can shift the dielectric material between the two plates, changing the overall dielectric constant. The dielectric change is depicted in fig.3. The equation describes the change in capacitance produced by a change in the dielectric constant:

$$\Delta C = (\Delta\varepsilon) \frac{lb}{d} . \quad (4)$$

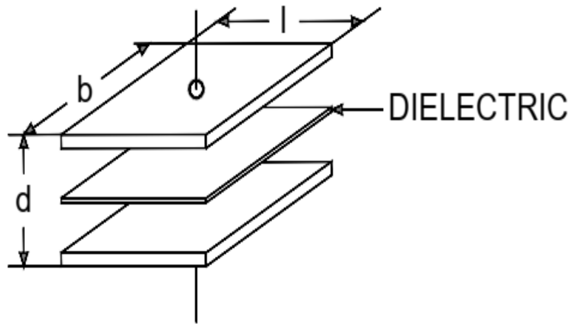


**Fig. 3 Capacitive sensor by changing the displacing of the dielectric material**

The planer type capacitive pressure is non-linear in characteristics [5]-[9]. Many researchers designed more complicated structures, such as a comb drive structure [10]-[14] or a touch mode capacitive sensor, which can be constructed to improve the sensitivity of such a simple capacitive sensor [15]-[20]. This paper proposes a capacitive pressure sensor with a comb drive structure featuring inter-digitated fingers that resemble two combs interlocking. This structure increased the surface area of the structure, which improved the capacitance of the sensor.

Developing a CDCPS necessitates a number of steps. First, the pressure must be translated into displacement, which can be done with the help of a diaphragm [21]-[22]. The displacement must then be transferred into one of the moving comb plate constructions using a mechanical coupler. As a result of the movement, the overlapping area of the comb plate structure altered, resulting in a change in capacitance, which is the sensor's output.

## 2. Proposed Design Flow

The proposed methodology in this study involves measuring the deflection of the circular diaphragms to calculate the sensor's output capacitance throughout a pressure range of 10 to 100 MPa. Then, using the COMSOL multiphysics simulator, simulate the sensor's 3D model with the same input range of 10 MPa to 100 MPa. After that, the computed and simulated deflection values are compared for circular diaphragms. Fig. 4 shows the proposed design flow for a comb-drive capacitive pressure sensor (CDCPS) based on a circular diaphragm with highly sensitive and linear.

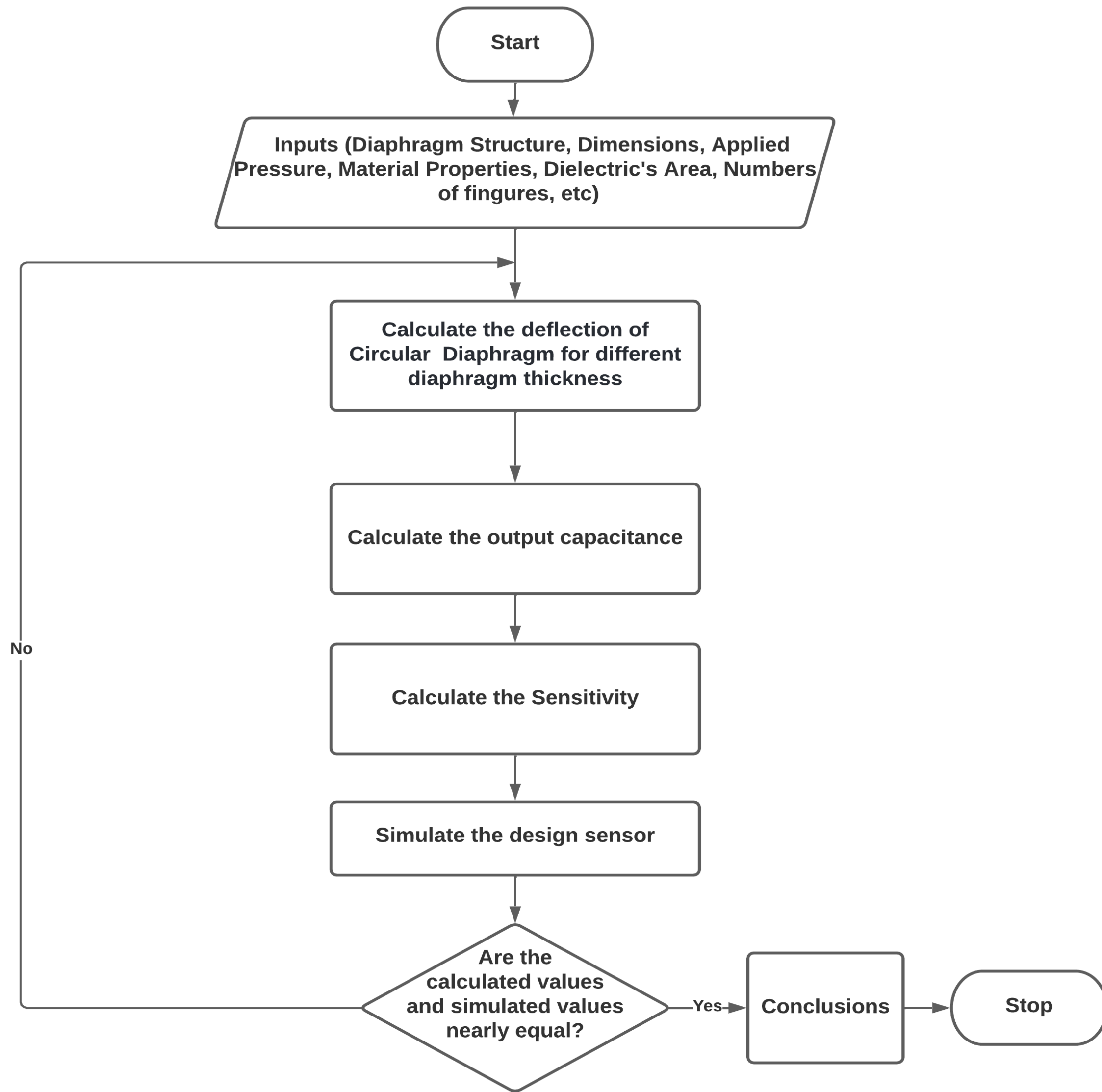


**Fig. 4 Design flow of a CDCPS based on a circular diaphragm**

## 3. Mathematical Modelling of the Sensor

The proposed model converts the mechanical input to an electrical output by the MEMS sensor. Mechanical and electrostatic modeling are the two parts of the mathematical modeling of such sensors. On the input side, mechanical modeling is done, and on the output side, electrostatic modeling is done. The mathematical model for a CDCPS has two main components. Their functions are summarized as follows:

### *3.1. Mechanical Modelling*

This comb drive 3D model includes a diaphragm, mechanical coupler, moving comb structure, and fixed comb structure, as shown in Fig. 5. The diaphragm's job is to convert pressure into displacement due to the applied pressure. The mechanical coupler converts diaphragm deflection into linear displacement by isolating the diaphragm and the comb structure. The comb structure converts the linear displacement into a change in capacitance between the moving and fixed comb plates.

The circular diaphragm is employed in this study; out of the two most typically used diaphragms, square and circular diaphragms. The pressure on the diaphragm's surface is treated as an evenly distributed load or pressure on the diaphragm because the sensor is small enough.

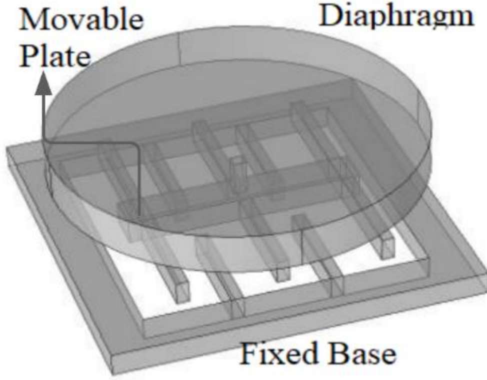


**Fig. 5 3D model of the circular diaphragm-based CDCPS**

The deflection is calculated as the circular diaphragm's applied pressure. Consider the diameter of a circular diaphragm with a thickness of $h$ and a diameter of $2a$. The differential equation of a circular diaphragm under pressure is given in [23]-[15] as

$$\frac{1}{r}\frac{d}{dx}r\frac{d}{dx}\left[\frac{1}{r}\frac{d}{dx}r\frac{d}{dx}w(r)\right]=\frac{P}{D}, \tag{5}$$

where D is the flexure rigidity of the diaphragm, w is the deflection function of the circular diaphragm, P is the applied pressure, and r is the distance from the edge.
The value of flexure rigidity is given by

$$D=\frac{Eh^3}{12(1-v^2)}, \tag{6}$$

Where $E$ is the Young's Modulus, $v$ is the Poisson's Ratio of the diaphragm material.

The differential function of a circular diaphragm can be written as

$$\begin{aligned} w(r) &= \frac{P}{D}\int\frac{1}{r}\int r\int\frac{1}{r}\int rdrdrdrdr \\ &= \frac{P}{D}\frac{r^4}{64}+K_1r^2\ln r+K_2r^2+K_3\ln r+K_4 \end{aligned} \tag{7}$$

where $K_1$ $K_2$ $K_3$, and $K_4$ are arbitrary constants.

Since the natural logarithm of zero does not exist at $w(0)=0$, otherwise, the constants $K_1$ and $K_3$ should be zero separately

$$w(r)=\frac{P}{D}\frac{r^4}{64}+K_2r^2+K_4. \tag{8}$$

Whereas the condition: $\frac{\partial w(r)}{\partial r}=0$ at $r=a$ is satisfied by eqn. (8), which implies

$$\frac{\partial w(r)}{\partial r}=\frac{4P}{D}\frac{r^3}{64}+2rK_2=0 \ ,$$

$$K_2=-\frac{P}{D}\frac{a^2}{32}. \tag{9}$$

Now, putting the value of $K_2$ into the equation (8) and using the condition: $w(a)=0$ at $x=a$, we have

$$w(a)=\frac{P}{D}\frac{a^4}{64}+K_2a^2+K_4,$$

$$0=\frac{P}{D}\frac{a^4}{64}-\frac{P}{D}\frac{a^2}{32}a^2+K_4,$$

$$K_4=\frac{P}{D}\frac{a^4}{64}. \tag{10}$$

Using the values of $K_2$ and $K_4$ into equation no. (8) we get finally

$$\begin{aligned} w(r) &= \frac{P}{D}\frac{r^4}{64}-\frac{P}{D}\frac{a^2}{32}r^2+\frac{P}{D}\frac{a^4}{64} \ , \\ &= \frac{P}{64D}(a^2-r^2)^2. \end{aligned} \tag{11}$$

Now putting the value of D in the above equation (11), then we get

$$\begin{aligned} w(r) &= \frac{12P(1-v^2)}{64Eh^3}(a^2-r^2)^2 \ , \\ &= \frac{0.1875P(1-v^2)}{Eh^3}(a^2-r^2)^2 \ . \end{aligned} \tag{12}$$

It is found that the maximum deflection of the circular diaphragm is found at $r=0$. Now

$$w(r)=\frac{0.1875Pa^4(1-v^2)}{Eh^3}. \tag{13}$$

We see that the deflection of the square diaphragm is influenced by the applied pressure, length, Poisson's ratio of the material, Young's modulus, and thickness.

### *3.2. Electrostatic Modeling*

The capacitance of the comb drive structure is varied following the displacement changes in any direction, such as length, breadth, and height. For the comb drive system, as shown in fig.6, the change in capacitance is given by

$$\Delta C = 4\Delta C_2 + 6\Delta C_1 . \tag{14}$$

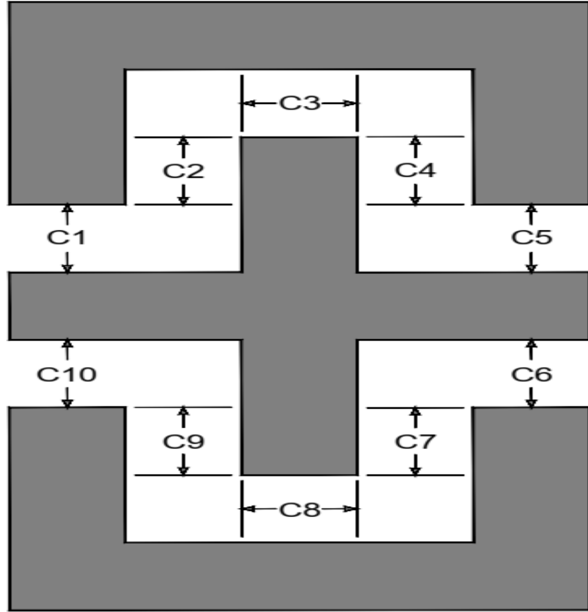


**Fig. 6 Simple comb drive structure**.

The capacitance changes when the depth of overlapping changes due to deflection in the particular design of the comb drive structure as:

$$\Delta C_1 = \varepsilon_0 \frac{b_1 w}{d},$$

$$\Delta C_2 = \varepsilon_0 \frac{l_2 w}{d},$$

$$\Delta C = 4\varepsilon_0 \frac{l_2 w}{d} + 6\varepsilon_0 \frac{b_1 w}{d}, \tag{15}$$

Where $w$ is the change in overlapping due to deflection produced by applied pressure, $P$, $b_1$, and $l_2$ are the breadth and length of the capacitor $C_1$ and $C_2$, respectively, and $\varepsilon_0$ is the absolute permittivity. The change in capacitance also increases if a factor of "n extends the interdigital of the comb structure."

$$\Delta C_n = 4n(\varepsilon_0 \frac{l_2 w}{d} + \varepsilon_0 \frac{b_1 w}{d}) + 2\varepsilon_0 \frac{b_1 w}{d}. \tag{16}$$

The sensitivity (S) of the sensor will be given by

$$S = (4n(\varepsilon_0 \frac{l_2 w}{d} + \varepsilon_0 \frac{b_1 w}{d}) + 2\varepsilon_0 \frac{b_1 w}{d}) / P. \tag{17}$$

The overall sensitivity is determined by the number of interdigital comb structures, capacitance length and width, overlapping depth due to displacement, and absolute permittivity.

## 4. Design and Simulation

The COMSOL multiphysics simulator is used to simulate the 3D model of the CDCPS. Gold (Au) is used for the diaphragm, silicon dioxide ($SiO_2$) for the mechanical coupler, and Au is used for the moveable and fixed comb structure. The radius of the diaphragm is 300 µm. Simulation is performed for different diaphragm thicknesses of 25 µm, 30 µm, 35 µm, and 40 µm. The various observations are made from the input range of 10 MPa to 100 MPa. The dimension of the comb dive taken for simulation is shown in fig. 7.

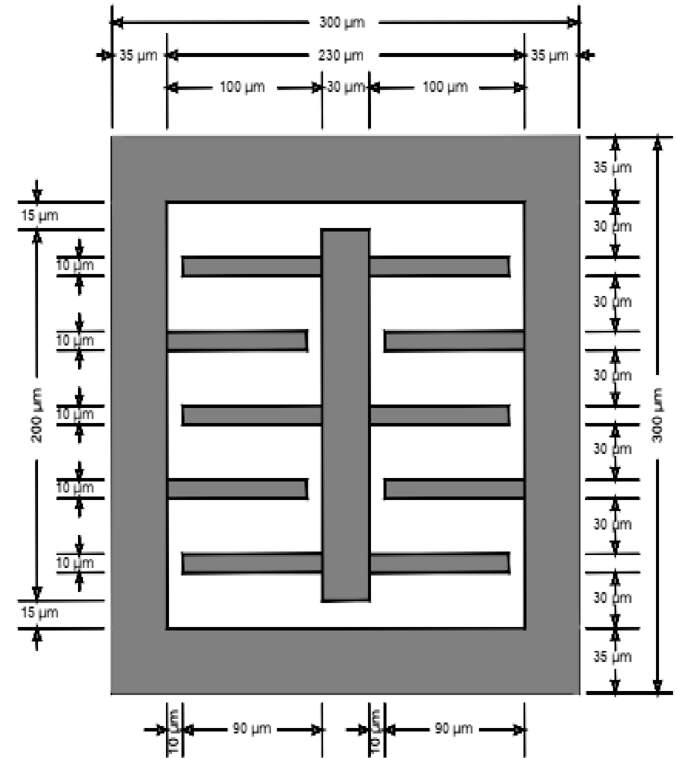


**Fig. 7 Dimension of the comb structure used for simulation**

The simulated deflection output of a sensor for a circular diaphragm with a thickness of 25 m at 100 MPa is shown in Figure 8. Table 1 shows the output deflections of all simulations and calculated values for various diaphragm thicknesses in the input range of 10 MPa to 100 MPa.

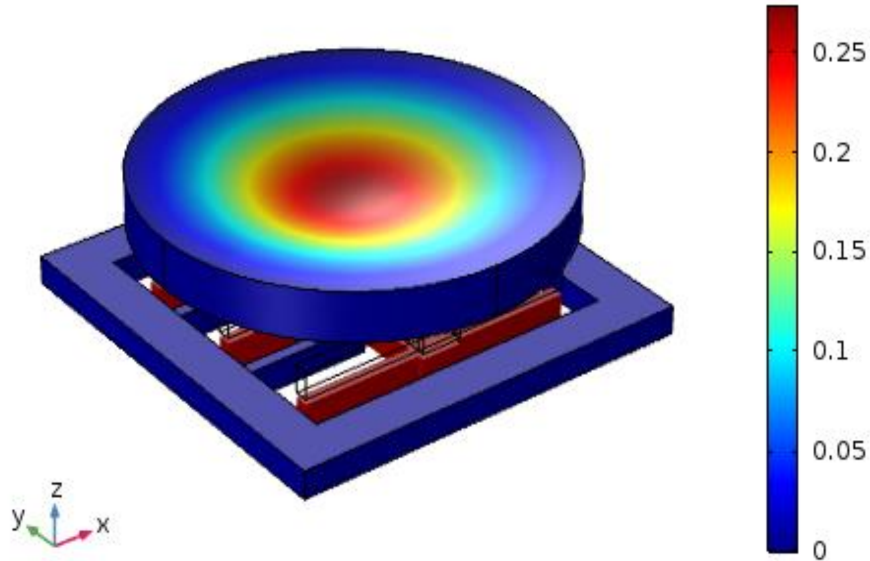


**Fig. 8 Displacement of the circular diaphragm**

**Table 1. Simulated vs. calculated displacements for circular diaphragm with different diaphragm thickness**

| Pressure (MPa) | 25 µm (µm) | | 30 µm (µm) | | 35 µm (µm) | | 40 µm (µm) | |
|---|---|---|---|---|---|---|---|---|
| | **Sim** | **Cal** | **Sim** | **Cal** | **Sim** | **Cal** | **Sim** | **Cal** |
| 10 | 0.67 | 0.61 | 0.40 | 0.35 | 0.27 | 0.23 | 0.20 | 0.15 |
| 20 | 1.33 | 1.22 | 0.82 | 0.70 | 0.55 | 0.46 | 0.39 | 0.3 |
| 30 | 2.00 | 1.83 | 1.22 | 1.06 | 0.82 | 0.69 | 0.59 | 0.45 |
| 40 | 2.66 | 2.44 | 1.63 | 1.41 | 1.09 | 0.92 | 0.79 | 0.6 |
| 50 | 3.31 | 3.05 | 2.04 | 1.77 | 1.37 | 1.15 | 0.99 | 0.75 |
| 60 | 3.96 | 3.66 | 2.44 | 2.12 | 1.64 | 1.38 | 1.19 | 0.9 |
| 70 | 4.56 | 4.27 | 2.84 | 2.47 | 1.91 | 1.61 | 1.38 | 1.05 |
| 80 | 5.23 | 4.88 | 3.25 | 2.83 | 2.18 | 1.84 | 1.58 | 1.2 |
| 90 | 5.85 | 5.49 | 3.65 | 3.18 | 2.45 | 2.07 | 1.78 | 1.35 |
| 100 | 6.46 | 6.11 | 4.04 | 3.54 | 2.73 | 2.3 | 1.98 | 1.5 |
| Sim = Simulated Values | | Cal = Calculated Values | | | | | | |

The graphical representation of Table 1 above is shown in Fig. 9. Table 1. summarizes the simulated and computed output displacements for the proposed circular diaphragm-based comb-drive capacitive pressure sensors. This table also shows that the diaphragm deflection rises as the diaphragm thickness increases.

The deflection of the circular with a thickness of 25 µm is larger, and their simulated and calculated values are relatively similar. The displacement of the diaphragm is highly linear to the applied pressure, as shown in this diagram. This diagram also shows that lower diaphragm thickness results in greater sensor deflection, whereas higher diaphragm thickness results in less deflection. The simulated and computed displacement values are likewise quite close, as shown in the figures.

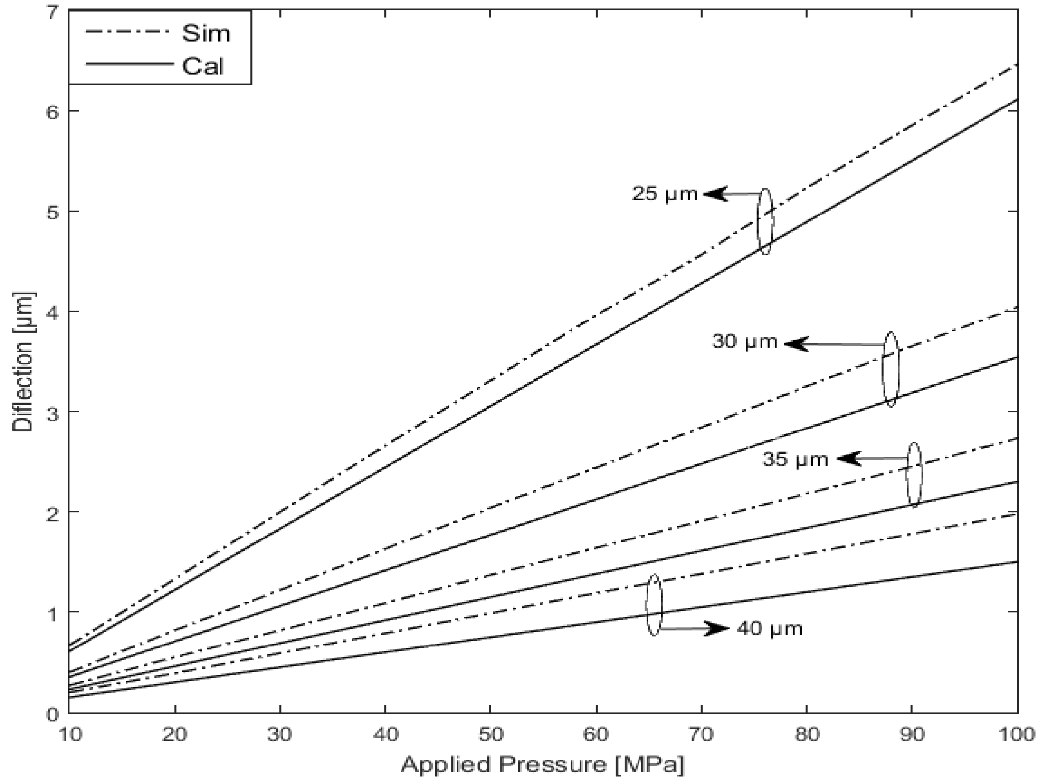


**Fig. 9 Simulated and calculated displacements of the circular diaphragm**

Table 2 lists the simulated and computed output capacitances for the proposed CD-CDCPS. The table demonstrates that the diaphragm with the smallest thickness has the most capacitance change.

**Table 2. Simulated vs. Calculated change in capacitance for circular diaphragm-based comb drive pressure sensor**

| Pressure (MPa) | 25 µm (fF) | | 30 µm (fF) | | 35 µm (fF) | | 40 µm (fF) | |
|---|---|---|---|---|---|---|---|---|
| | Sim | Cal | Sim | Cal | Sim | Cal | Sim | Cal |
| 10 | 0.19 | 0.23 | 0.12 | 0.13 | 0.07 | 0.08 | 0.06 | 0.05 |
| 20 | 0.39 | 0.47 | 0.24 | 0.27 | 0.15 | 0.17 | 0.12 | 0.11 |
| 30 | 0.59 | 0.70 | 0.37 | 0.40 | 0.24 | 0.25 | 0.18 | 0.17 |
| 40 | 0.79 | 0.94 | 0.49 | 0.54 | 0.32 | 0.34 | 0.24 | 0.22 |
| 50 | 0.99 | 1.17 | 0.61 | 0.68 | 0.40 | 0.43 | 0.30 | 0.28 |
| 60 | 1.18 | 1.41 | 0.73 | 0.81 | 0.48 | 0.51 | 0.36 | 0.34 |
| 70 | 1.37 | 1.64 | 0.89 | 0.95 | 0.56 | 0.60 | 0.42 | 0.39 |
| 80 | 1.56 | 1.88 | 0.98 | 1.08 | 0.65 | 0.68 | 0.48 | 0.45 |
| 90 | 1.74 | 2.11 | 1.09 | 1.22 | 0.73 | 0.77 | 0.53 | 0.51 |
| 100 | 1.91 | 2.35 | 1.21 | 1.36 | 0.81 | 0.86 | 0.59 | 0.57 |

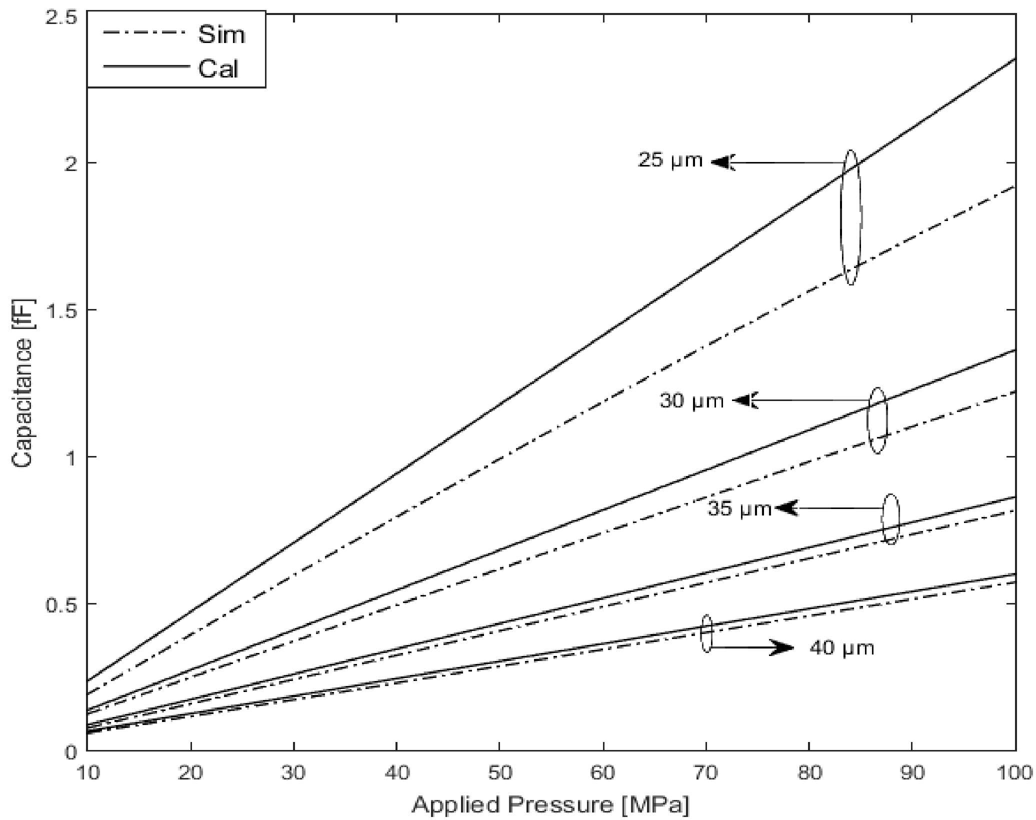


.

**Fig. 10 Simulated and calculated change in capacitance of circular diaphragm**

Table 2 is represented graphically in Fig. 10. The change in capacitance output is highly linear with the applied pressure, as shown in this diagram. This also demonstrates that the calculated and simulated capacitance changes are fairly similar.

The sensitivity of the 25 µm circular diaphragm-based comb-drive capacitive pressure for simulated and calculated is 0.192 fF/MPa and 0.235 fF/MPa, respectively, as shown in this figure.

## 5. Conclusion

This part of the research study focuses on the mathematical modeling and simulation of the comb drive pressure sensor for sensing pressure ranges of 10 MPa to 100 MPa. A diaphragm-based comb-drive capacitive pressure sensor is presented and developed using a design technique. As the simulated and computed values are found so close, the proposed design flow can be employed in the future. As the diaphragm thicknesses drop, the sensitivity improves. As the diaphragm length rises, the sensor's sensitivity increases. Young's modulus and Poisson's ratio positively impact the sensor's sensitivity. As the length, breadth, and number of comb driving fingers increase, capacitance changes. As the distance between the plates shrinks, the sensor's sensitivity improves. Finally, a linear output characteristic sensor is developed. It is found that the sensitivity of the circular diaphragm-based comb-drive capacitive pressure for simulated and calculated is 0.192 fF/MPa and 0.235 fF/MPa, respectively, for diaphragm thickness of 25 µm.

## Conflicts of Interest

The authors declare that there is no conflict of interest regarding the publication of this paper.

## Acknowledgment

The authors would like to thank the authority of Rajiv Gandhi University, Arunachal Pradesh, India, for the constant support and appreciation received during the preparation of the research work. All the authors contributed equally to this work.

## References


[1] M. Molla-Alipour and B. A. Ganji, Analytical analysis of mems capacitive pressure sensor with circular diaphragm under dynamic load using differential transformation method (DTM), Acta Mechanica Solida Sinica, 28(4) (2015) 400–408. doi: 10.1016/S0894-9166(15)30025-2.

[2] V. Rochus, B. Wang, H. A. C. Tilmans, A. Ray Chaudhuri, P. Helin, S. Severi, X. Rottenberg, Fast analytical design of MEMS capacitive pressure sensors with sealed cavities, Mechatronics, 40 (2016) 244–250.doi: 10.1016/j.mechatronics.2016.05.012.

[3] J. I. Yoon, K. S. Choi, and S. P. Chang, A novel means of fabricating microporous structures for the dielectric layers of a capacitive pressure sensor, Microelectronic Engineering, 179 (2017) 60–66.doi: 10.1016/j.mee.2017.04.028.

[4] Y. Lian, J. Sun, X. Ge, Z. Yang, X. He, and Z. Zheng, A theoretical study of an improved capacitive pressure sensor: Closed-form solution of uniformly loaded annular membranes, Measurement, 111 (2017) 84–92.doi: 10.1016/j.measurement.2017.07.025.

[5] Z. Guo, T. Zhang, F. Zhou and F. Yu, Design and Experiments for a Kind of Capacitive Type Sensor Measuring Air Flow and Pressure Differential, IEEE Access, 7 (2019) 08980-108989.doi: 10.1109/ACCESS.2019.2933485.

[6] T. Chen, J. Chiu, C. Cheng and M. S. Lu, Design and Characterization of Capacitively Sensed Squeeze-Film Pressure Sensors, IEEE Sensors Journal, 19(5) (2019) 1653-1660.doi: 10.1109/JSEN.2018.2883477.

[7] A. Madupu, A. Sharma, P. Gowri Ishwari, and S. Ijjada, Analysis and enhancement of capacitive pressure sensor's sensitivity through material engineering processes, Materials Today: Proceedings, (2020).doi: 10.1016/j.matpr.2020.10.287.

[8] S. K. Jindal, K. Sethi, I. Patel, A. Kumar, and S. K. Raghuwanshi, A Semi-Analytical and Computationally Efficient Method to Calculate the Touch-Point Pressure and Pull-In Voltage of a MEMS Pressure Sensor With a Circular Diaphragm, IEEE Sensors Journal, 21(2) (2021) 1332-1339.doi: 10.1109/JSEN.2020.3019205.

[9] X. Tang, Q. Gu, P. Gao, and W. Wen, "Ultra-sensitive wide-range small capacitive pressure sensor based on porous CCTO-PDMS membrane," Sensors and Actuators Reports, 3 (2021) 10002.doi: 10.1016/j.snr.2021.100027.

[10] G. Blasquez, X. Chauffleur, P. Pons, C. Douziech, and P. F. P. Menini, Thermal Drift and Chip Size in Capacitive Pressure Sensors, Eurosensors 13 (1999) 461-464. https://hal.laas.fr/hal-02170328/document

[11] W. H. Ko and Q. Wang, Touch mode capacitive pressure sensors, Sensors, and Actuators A: Physical, 75(3) (1999) 242–251.doi: 10.1016/S0924-4247(99)00069-2.

[12] S. Guo, J. Guo, and W. H. Ko, A monolithically integrated surface micromachined touch mode capacitive pressure sensor, Sensors, and Actuators A: Physical, 80(3) (2000) 224–232.doi: 10.1016/S0924-4247(99)00344-1.

[13] A. Preethi and L. Chitra, Comparative analysis of materials for designing a highly sensitive capacitive type of MEMS pressure sensor, IEEE National Conference on Emerging Trends in New Renewable Energy Sources and Energy Management (NCET NRES EM), (2014) 1–8. doi: 10.1109/NCETNRESEM.2014.7088730.

[14] Liu, Y. Pan, P. Wu, L. Du, Z. Zhao, and Z. Fang, A novel capacitive pressure sensor based on non-coplanar comb electrodes, Sensors and Actuators A: Physical, 297 (2019) 111525.doi: 10.1016/j.sna.2019.07.049

[15] S.-P. Chang, J.-B. Lee, and M. G. Allen, Robust capacitive pressure sensor array, Sensors, and Actuators A: Physical, 101(1)(2002) 231–238.doi: 10.1016/S0924- 4247(02)00193-0

[16] M.-X. Zhou, Q.-A. Huang, and M. Qin, Modeling, design, and fabrication of a triple-layered capacitive pressure sensor, Sensors, and Actuators A: Physical, 117(1) (2005) 71–81.doi: 10.1016/j.sna.2004.05.036.

[17] R. G. Azevedo, D. G. Jones, A. V. Jog, B. Jamshidi, D. R. Myers, L. Chen, X. Fu, M. Mehregany, M. B. J. Wijesundara, A. P. Pisano, A SiC MEMS Resonant Strain Sensor for Harsh Environment Applications, IEEE Sensors Journal, 7(4) (2007) 568–576.doi: 10.1109/JSEN.2007.891997.

[18] V. Tsouti, G. Bikakis, S. Chatzandroulis, D. Goustouridis, P. Normand, and D. Tsoukalas, Impact of structural parameters on the performance of silicon micromachined capacitive pressure sensors, Sensors, and Actuators A: Physical, 137(1) (2007) 20–24.doi: 10.1016/j.sna.2007.02.015.

[19] C.-C. Chiang, C.-C. K. Lin, and M.-S. Ju, An implantable capacitive pressure sensor for biomedical applications, Sensors, and Actuators A: Physical, 134(2) (2007) 382–388.doi: 10.1016/j.sna.2006.06.007.

[20] J. Han and M. A. Shannon, Smooth Contact Capacitive Pressure Sensors in Touch- and Peeling-Mode Operation, IEEE Sensors Journal, 9(3) (2009) 199–206.doi: 10.1109/JSEN.2008.2011090.

[21] S. M. Maibam, D. S. Aheibam and M. Swanirbhar, An Engineering Approach for Modeling and Design of a Diaphragm Based Comb Drive Capacitive Pressure Sensor, Proceedings of the 5th International Conference on Computers & Management Skills, NERIST, (2019),doi: http://dx.doi.org/10.2139/ssrn.3516732

[22] E. G. Bakhoum and M. H. M. Cheng, Capacitive Pressure Sensor With Very Large Dynamic Range, IEEE Transactions on Components and Packaging Technologies, 33(1) (2010) 79–83, doi: 10.1109/TCAPT.2009.2022949.

[23] S. P. Timoshenko and S. Woinowsky-Krieger, Theory of Plates and Shells, New York: McGraw Hill, (1959). ISBN: 0070647798.

[24] A. C. Ugural, Plates and shells: theory and analysis, Fourth edition, Boca Raton, London, New York, (2018). ISBN: 9781138032453.

[25] M. Bao, Analysis and Design Principles of MEMS Devices, Elsevier Science, (2005). ISBN 9780444516169.